HHS Public Access

Author manuscript

Cancer Res. Author manuscript; available in PMC 2022 October 15.

Published in final edited form as:

Cancer Res. 2022 April 15; 82(8): 1575–1588. doi:10.1158/0008-5472.CAN-21-2778.

Ketogenesis attenuates KLF5-dependent production of CXCL12 to overcome the immunosuppressive tumor microenvironment in colorectal cancer

Ruozheng Wei[1,2], **Yuning Zhou**[2], **Chang Li**[2], **Piotr Rychahou**[2,3], **Shulin Zhang**[2,4], **William B. Titlow**[2,4], **Greg Bauman**[5], **Yuanyuan Wu**[2], **Jinpeng Liu**[2], **Chi Wang**[2], **Heidi L. Weiss**[2], **B. Mark Evers**[2,3], **Qingding Wang**[2,3]

[1]Department of Pancreatic Surgery, Union Hospital, Tongji Medical College, Huazhong University of Science and Technology, Wuhan 430022, China

[2]Markey Cancer Center, University of Kentucky, Lexington, KY, 40536, USA

[3]Department of Surgery, University of Kentucky, Lexington, KY, 40536, USA

[4]Department of Pathology and Laboratory Medicine, University of Kentucky, Lexington, KY, 40536, USA

[5]Department of Microbiology, Immunology & Molecular Genetics, University of Kentucky, Lexington, KY, 40536, USA

Abstract

The dynamic composition of the tumor microenvironment (TME) can markedly alter the response to targeted therapies for colorectal cancer (CRC). Cancer associated fibroblasts (CAF) are major components of TMEs that can direct and induce infiltration of immunosuppressive cells through secreted cytokines such as CXCL12. Ketogenic diets (KD) can inhibit tumor growth and enhance the anticancer effects of immune checkpoint blockade. However, the role of ketogenesis on the immunosuppressive TME is not known. Here, we show that decreased ketogenesis is a signature of CRC and that an increase in ketogenesis using a KD decreases CXCL12 production in tumors, serum, liver, and lungs. Moreover, increasing ketogenesis by overexpression of the ketogenic enzyme 3-hydroxy-3-methylglutaryl-CoA synthase 2 (HMGCS2) or treatment with the ketone body β-hydroxybutyrate markedly decreased expression of KLF5, which binds the CXCL12 promoter and induces CXCL12 expression in CAFs. KD decreased intratumoral accumulation of immunosuppressive cells, increased infiltration of NK and cytotoxic T cells, and enhanced the anticancer effects of PD-1 blockade in murine-derived CRC. Furthermore, increasing ketogenesis

[#]**Correspondence:** Qingding Wang, Ph.D., M.D., Markey Cancer Center, University of Kentucky, 800 Rose Street, Lexington, KY 40536-0293, Phone: (859) 323-4382; qingding.wang@uky.edu or B. Mark Evers, M.D., Markey Cancer Center, University of Kentucky, 800 Rose Street, 181 Chandler Hospital, Lexington, KY 40536-0293, Phone: (859) 323-6556; mark.evers@uky.edu.

Author contributions: RW performed most experiments and summarized data with the help from QW. YZ contributed to IHC staining. CL contributed to plasmid construction of CXCL12 promoter, constructing inducible HMGCS2 or HMGCS2-Mut overexpressing CAFs and performing *in vivo* experiments. PR contributed to the metastasis assessment. SZ and WT contributed to performing scRNA-seq. GB contributed to flow cytometric analysis. YW, JL and CW contributed to RNA-seq data analysis. HLW contributed to experimental design and data analysis. QW and BME conceived the project, supervised the research, designed experiments, analyzed data, prepared figures, and drafted the manuscript.

Conflict of Interest: The authors declare no potential conflicts of interest.

inhibited CRC migration, invasion, and metastasis in vitro and in vivo. Overall, ketogenesis is downregulated in the CRC TME, and increased ketogenesis represses KLF5-dependent CXCL12 expression to improve the immunosuppressive TME, which leads to the enhanced efficacy of immunotherapy and reduced metastasis. Importantly, this work demonstrates that downregulation of de novo ketogenesis in the TME is a critical step in CRC progression.

Keywords

Colorectal cancer; ketogenesis; CXCL12; tumor microenvironment; KLF5

Introduction

Despite significant improvements in the treatment of colorectal cancer (CRC), the prognosis for CRC patients with metastasis remains dismal with a median overall survival of approximately 30 months (1). Immunotherapy such as immune checkpoint blockade (ICB) represents a novel therapeutic approach for a variety of cancers including CRC with microsatellite instability-high (MSI-H) (2). However, ICB therapy shows little or no clinical activity in the majority of patients with microsatellite-stable (MSS) CRC (2). The tumor microenvironment (TME) has a dynamic composition that affects the efficacy of targeted therapies for CRC (3). Critical interactions between cancer cells occurring in the TME mostly promote tumor initiation, resistance, metastasis and recurrence (3). Therefore, to achieve an increase in survival, efficient strategies are needed for disruption of these interactions in the TME (4).

Accumulation of cancer-associated fibroblasts (CAFs) in TME is associated with poor prognosis and recurrence of CRC (5). CAFs within the TME have shown to be an important determinant of the tumor immune response (6). The chemokine CXCL12, also known as stromal cell–derived factor-1 (SDF1), is expressed in the TME mainly by CAFs (7). CXCL12 protein, which binds to G protein-coupled receptors CXCR4 and CXCR7, promotes tumor immunosuppression by recruiting specific immune cell populations (8). Activation of the CXCL12/CXCR4 axis is common in many solid tumors and contributes to tumor immunosuppression and metastasis (9). The factors controlling the level of CXCL12 in TME remains largely undefined.

Ketogenic diets (KDs), which have high-fat and low-carbohydrate content, have been demonstrated to be a safe and achievable component in the treatment regimen of some cancers (10). Recent studies showed that a KD inhibits growth of certain tumor xenografts *in vivo* and enhances anticancer effects of ICB in murine CRC, melanoma, renal, and non-small cell lung cancer orthotopic tumor models (11,12). However, the dynamics of ketogenesis and the role of ketogenesis on the immunosuppressive TME are not known.

Our recent studies demonstrate that an increase in ketogenesis induces differentiation and inhibits CRC cell glycolysis (13,14). In addition, we showed that inhibition of WNT/β-catenin or mTOR signaling increases the expression of the ketogenic enzyme 3-Hydroxy-3-Methylglutaryl-CoA Synthase 2 (HMGCS2) and the production of the ketone body beta-hydroxybutyrate (βHB) in CRC cells (13,14). Here, we show that decreased ketogenesis is

a signature of CRC and that an increase in ketogenesis represses KLF5-dependent CXCL12 expression and thus inhibits immunosuppressive TME, enhances the anticancer effects of PD-1 blockade and inhibits lung metastasis. Importantly, our study demonstrates that downregulation of *de novo* ketogenesis in the TME is a critical step in CRC progression and suggest a potential benefit of using KD to combat CRC immunoresistance and metastasis.

Materials and Methods

Animal studies

C57BL/6J and BALB/cJ mice (female, 6-week-old) were obtained from The Jackson Laboratory. All animal procedures were conducted with approval and in compliance with University of Kentucky Institutional Animal Care and Use Committee. Mice were housed in a pathogen-free environment on a 12-hour light/dark cycle and received a normal chow diet or KD (F3666, Bio-serv) with free access to drinking water.

MC38 or CT26 tumors were established by subcutaneously injecting cells (0.5×10^6 cells in 50% matrigel in PBS, 100 μL/mouse) into the right flank of either C57BL/6J or BALB/cJ female mice. Tumor sizes were measured every 2–3 days by caliper after implantation and tumor volume was calculated in mm^3 ($mm^3 = \pi/6 \times (\text{larger diameter}) \times (\text{smaller diameter})^2$). Four days after tumor cell implantation (mean tumor volume reached approximately 100 mm^3), animals were pooled and randomly divided into designated experimental groups with comparable average tumor size and body weight. For ketogenic/anti-PD-1 combination treatment, mice were grouped into IgG control [normal diet (NC) + IgG isotype control (BE0089, Bio-XCell)], ketogenic treatment (KD + IgG isotype control), anti-PD-1 antibody treatment [NC + anti-PD-1 monoclonal antibody (BE0146, Bio-XCell)] and anti-PD-1 antibody plus ketogenic treatment (KD + anti-PD-1). Anti-PD-1 antibody and IgG control treatments were conducted by intraperitoneal injection (200 μg per mouse in 100 μL PBS) every two days from day 5 for a total of 7 injections. For survival studies, C57BL/6J or BALB/cJ mice were monitored for tumor volume every 1–3 days after initial treatment until tumors became necrotic or their volume reached 2000 mm^3.

For the lung metastasis model, GFP-CT26 cells (1×10^6 cells per BALB/cJ mouse) were injected via tail vein as we have described (15). Two weeks after cancer cell injection the mice were euthanized, and lungs were removed to examine GFP fluorescence of metastatic tumors using a Lago (Spectral Instruments Imaging) equipped with an excitation source (465 nm) and emission filter (510 nm). GFP signal was quantified in Aura software (Spectral Instruments Imaging).

scRNA-seq

Single cell suspensions were prepared following the recommendations from 10X Genomics and $CD45^+$tumor-infiltrating leukocytes were enriched for single-cell analysis as described (16). Dead cells were removed from the single cell suspension using the Dead Cell Removal Kit (Miltenyi Biotec). $CD45^+$ leukocytes were magnetically labeled and enriched using magnetic beads (Miltenyi Biotec). Cells were stained with Trypan Blue and counted using Cuntess II FL (Invitrogen). Tumors from five different mice were pooled per diet

condition. Ten thousand cells were targeted for sequencing and loaded onto 10X Genomics Chromium Controller for Gel Beads-in-emulsion (GEMs) formation. Library was prepared was conducted according to the manufacturer's instructions. Single indexed, paired-end libraries were sequenced on an Illumina HiSeq2500 and data analyzed using Cell Ranger software (10X Genomics).

Flow cytometry

Collect 2×10^6 or fewer cells per tumor from single cell suspension and resuspend pellet in 50 μl PBS containing Fc blocking antibody (anti-mouse CD16/32, BioLegend) and fixable live/dead stain (Zombie UV™ Fixable Viability Kit, BioLegend), incubate sample at room temperature for 15 min. Following Fc blocking, add surface antibody (see Supplementary Table 1) mix and incubate at 4°C for 60 min. Cells were washed twice with FACS buffer (BioLegend) and resuspended in 200 μl buffer. For cell cycle analysis, cells were fixed with 70% ice-cold ethanol and resuspended in FxCycle Propidium iodide/RNase staining solution (Thermo Scientific). Flow cytometry was performed using standard protocol on CytoFLEX LX analyzer (Beckman Coulter) and analyzed with FlowJo software.

Cell culture, treatments and transfection

Primary human CRC CAFs (hCAF-05) (Neuromics, Cat# CAF05), CRC CAFs (hCAF-6231) (Cell biologics, Cat# HC-6231) and mouse CAFs (mCAF), isolated from subcutaneous tumors using a Tumor-associated Fibroblast Isolation Kit (Miltenyi Biotec) and identified by means of morphology and immunofluorescence staining for S100A4 using anti-S100A4 antibody (Abcam), were cultured in VitroPlus III, Low Serum Complete medium (Neuromics). Human CRC cell line HCT116, and mouse CRC cell line CT26 were obtained from the American Type Culture Collection (ATCC). HCT116 cells were maintained in McCoy's 5a supplemented with 10% FCS. Mouse CRC cell line MC38, purchased from Kerafast, was maintained in DMEM supplemented with 10% FCS, 2 mmol/L glutamine, 0.1 mmol/L nonessential amino acids, 1 mmol/L sodium pyruvate, and 10 mmol/L Hepes. All cell lines were tested for Mycoplasma contamination using a sensitive PCR-based Mycoplasma detection kit (Biovision) and were found to be negative. Mouse CRC cell line CT26 cell line was tested via short tandem repeat (STR) profiling for authentication in 2021 (LabCorp). Cell s were infected with adenovirus vectors encoding either GFP (Ad-GFP; Vector BioLabs) or human KLF5 (Ad-KLF5, SignaGen), or treated with βHB (Sigma) or ML-264 (MedChemExpress). Cells were transfected with either human KLF5, HDAC1, or nontargeting control siRNA SMARTpool (Dharmacon) by electroporation (Gene Pulser, Bio-Rad). GFP-CT26 cell line was established after transfection with GFP lentivirus as described (15). GFP-expressing CT26 cells were selected with 5 μg/ml of puromycin and enriched by two cycles of fluorescence-activated cell sorting.

To establish cell lines with inducible overexpression of HMGCS2, human HMGCS2 cDNA (RC208128, OriGene Technologies) was sub-cloned into the pCW57-GFP-2A-MCS lentiviral vector (Addgene). HMGCS2-C166A mutant, an enzymatic dead HMGCS2 (17), was generated from wild type HMGCS2 by site-directed mutagenesis using QuikChange II XL Site-Directed Mutagenesis Kit (Agilent) with the primers as described (Supplementary Table 2) (17). HMGCS2-C166A mutant was sequenced, and mutation was confirmed.

hCAF-05 or hCAF-6231 cells were infected with lentiviral particles containing empty control vector or construct encoding human HMGCS2 or MGCS2-C166A mutant, selected with puromycin (5 μg/ml), and induced by doxycycline (DOX) (400 ng/ml) for 48 h as previously described (18).

Cell growth assay

Cells (5×10^4/well) were seeded in 6-well plates in triplicate. Cell proliferation was analyzed by counting the number of viable cells in response to the treatment of βHB, HMGCS2 overexpression and knockdown or overexpression of KLF5 as described (19). Each experiment was repeated at least three times.

Western blot analysis

Total protein was resolved by SDS-PAGE and transferred to PVDF membranes, immunoblotted with specific primary and secondary antibodies (see Supplementary Table 1) as we have described previously (13). α-SMA signals from 10 paired human tissues was quantitated densitometrically and expressed as fold change to β-actin.

Quantitative real time RT-PCR analysis

Total RNA was extracted using RNeasy Mini Kit (QIAGEN) and DNase-treated. Synthesis of cDNA was performed a High Capacity cDNA Reverse Transcription Kit (Applied biosystems). The TaqMan probe and primers for human CXCL12, KLF5 and GAPDH were purchased from Thermo Scientific. Quantitative real time RT-PCR analysis was performed using TaqMan universal PCR master mix (Thermo Scientific) as described previously (13).

Clinical samples

Frozen fresh human tissue samples were collected from patients who previously had resections at UK Markey Cancer Center with informed consent and institutional IRB approval (IRB#13–0753-P2H). Paraffin-embedded tissues were obtained from Markey's tissue repository. The frozen samples were "snap-frozen" in liquid nitrogen and stored at −80°C. The frozen fresh human tissue samples included 13 paired primary colorectal tumor and adjacent normal colon tissues. The paraffin-embedded tissues included 5 paired primary colorectal tumor, adjacent normal colon, and liver metastases.

Immunohistochemistry (IHC)

IHC staining was performed as described previously (19). Tissue was processed for routine IHC staining using the following antibodies: anti-CXCR7/RDC-1 and anti-CXCR4 (R&D systems), Anti-SDF1 and anti-HMGCS2 (Abcam), and anti-BTEB2 (KLF5). Negative controls (including no primary antibody or isotype-matched mouse immunoglobulin G) were used in each assessment.

βHB assay

Intracellular and plasma βHB concentration was determined using a Beta-Hydroxybutyrate Assay Kit (Sigma Aldrich) according to the manufacturer's protocol. Each plotted value

was normalized to total amount of protein used from cell lines and tissues or volume from plasma.

ELISA of SDF-1

SDF-1 concentrations of cell lysates, cell medium, plasma or tissues were analyzed using SDF-1 alpha/CXCL12A Human/Mouse ELISA Kits (Thermo Scientific). All the assays were performed according to the protocols provided by the manufacturer. Each plotted value was normalized to total amount of protein used from cell lysates and tissues or volumes from media and plasma.

Chromatin immunoprecipitation (ChIP) analysis

hCAF-05 with empty vector or construct expressing HMGCS2 were seeded and treated with DOX (400 ng/mL) for 48 h to induce HMGCS2 expression before lysis. ChIP Assay was performed using the ChIP-IT High Sensitivity® kit (Active motif) in accordance with the manufacturer's protocol as we have described previously (19). The human CXCL12 promoter region containing the KLF5 binding site was amplified by PCR from total (input) or immunoprecipitated chromatin using the primers as described in Supplementary Table 2.

CXCL12 promoter cloning and dual-luciferase assay

Genomic DNA from hCAF-05 cells was extracted. CXCL12 gene promoter fragments 1070 bp (from −970 bp to +100 bp from the transcription start site), 944 bp (−844 bp to +100 bp) and 767 bp (−667 to +100 bp) were produced by PCR using primers containing *NheI* and *HindIII* restriction sites as described in Supplementary Table 2. The primers were synthesized based on the genomic sequence lying upstream of the human CXCL12 cDNA (NCBI, NC_000010.11). PCR products were cloned into the reporter vector (pGL3-basic), sequenced, and confirmed to contain contiguous genomic sequences. The pRL-Tk-luc plasmid was co-transfected together with CXCL12 promoter constructs to normalize for variation in transfection efficiency. Luciferase assays were performed as previously described (18).

Transwell migration and invasion assay

Migration assays were performed in chambers coated with collagen I (Thermo Scientific). Invasion assays were performed in chambers coated with Matrigel, as instructed by the manufacturer (BD Biosciences). Briefly, HCT116 cells were incubated in serum free medium for 24 h. Cells in serum free medium were seeded 5×10^4/well into the upper chamber of the 24-well Transwell plate (Corning, Inc.). 600 μl conditioned medium was introduced to the lower wells and cultured for 6 h. The number of migrated cells were counted in five areas at 200x magnification using an inverted microscope as described (20). A similar procedure was carried out to detect the invasion ability of HCT116 cells except for using the chambers being coated with Matrigel and cultured for 24 h.

Quantification and statistical analysis

For *in vitro* experiments and *in vivo* studies, pairwise comparisons between 2 groups were performed using two-sample t test or analysis of variance for multiple groups with contrast

statements. Adjustments for multiple testing between groups within an experiment were performed using Holm P adjustment method. Kaplan-Meier curves were estimated for survival of *in vivo* studies and compared using the log-rank test. All data from animal samples with measurement of study endpoints were included in the analysis. Raw sequence reads from scRNA-seq data were processed and aligned to the GRCm38 (2020-A) mouse reference transcriptome using the Cell Ranger v6.0.0 pipeline (10X Genomics) with default parameters. The gene expression matrices were processed using scDblFinder (v1.1.8) R package for doublets prediction and removal.

All materials generated in this study are available from the corresponding author, Qingding Wang (qingding.wang@uky.edu). The scRNA-seq data reported in this study is available from Gene Expression Omnibus (GEO) with accession code GSE180110. All other data are available from the corresponding author (Qingding Wang) upon reasonable request.

Results

KD reduces the accumulation of immunosuppressive cells and increases the population of NK and T cells in the TME

We have previously shown that an increase in ketogenesis contributes to CRC cell differentiation (13). To determine whether an increase in ketogenesis affects the proliferation of CRC cells, we treated human CRC cell lines HCT116, DLD1, LS174T and RKO and mouse colon cancer cell lines MC38 and CT26 with βHB. Treatment with βHB (5 mM or 10 mM) for 3 days had minor effects on the proliferation of these cells (Supplementary Fig. 1A&B). To further determine the role of ketogenesis in CRCs, we next analyzed the antitumor effects of a KD using MC38 xenograft models in immune competent C57BL/6J mice (Fig. 1A&B) and athymic nude mice (Supplementary Fig. 1C). As shown in Fig. 1B, MC38 tumor grew slower in C57BL/6J mice fed KD compared to mice fed NC. In contrast, KD showed minor effects on MC38 tumor growth in athymic nude mice (Supplementary Fig. 1C), suggesting that the reduction in tumor growth by KD may be due to the altered immunosuppressive TME. To test this hypothesis, we used flow cytometry to profile tumor-infiltrating T cell and macrophage populations in MC38 tumors in immune competent C57BL/6J mice. We found that feeding tumor-bearing mice with a KD changes the immune landscape of MC38 tumors. Tumor tissues from mice fed a KD contained more T cells as a fraction of the $CD45^+$ leukocyte infiltrate (Fig. 1C). Specifically, increased infiltration of $CD8\alpha^+$ T cells were noted in KD tumors (Fig. 1D&E). In contrast, the percentage of total macrophages, especially immunosuppressive M2 macrophages, in the $CD45^+$ leukocyte infiltrate decreased with KD (Fig. 1F&G). Our results suggest a potential role for ketogenesis in the inhibition of the immunosuppressive TME in CRCs.

To further determine KD-induced alterations in tumor-infiltrating immune populations, we used single cell RNA sequencing (scRNA-seq) of tumor-infiltrating $CD45^+$ leukocytes to map the tumor immune transcriptional landscape in an unbiased and comprehensive manner (Fig. 1H–K). Mice with MC38 tumors were fed with NC or KD as described (Fig. 1A) and $CD45^+$ leukocytes in tumors were magnetically labeled and enriched by positive selection using CD45 MicroBeads. To define major cell populations, we performed unsupervised clustering analysis on integrated single-cell datasets from NC and KD tumors,

which identified 11 distinct clusters (Fig. 1H), where each of the 11 clusters contained cells from both diet conditions. We annotated clusters based on the expression of known genetic markers and categorized those cell populations into groups (see more details in Supplementary Fig. 2A–C and Supplementary Methods) (21,22). In agreement with the findings from flow cytometry analysis, increased $CD8^+$ T cell accumulation was found in tumors from mice fed a KD (Fig. 1I). Conversely, a marked decrease in total macrophage populations were found in KD tumors (16.8%) compared to NC tumors (30%). Moreover, significantly increased accumulation of natural killer (NK) cells was found in KD tumors (32.2%) compared to NC tumors (19.7%) (Fig. 1I). In addition, increased $CD4^+$ T cell populations were found in tumors from mice fed a KD. Further analysis demonstrated the increased percentage of anti-tumor conventional $CD4^+$ T cell population and decreased percentage of $CD4^+$ Treg population, which mediate tumor immunosuppressive functions (23), in total $CD4^+$ T cell populations of KD tumors (Fig. 1J). Tumor-infiltrating $CD8^+$ T cells and NK cells perform as effector cells against tumor cells (24). These data suggest an enhanced antitumor immune response in KD tumors. Moreover, reduced immunosuppressive populations was found in KD tumors as noted by the markedly decreased myeloid-derived suppressor cells (MDSCs) (Fig. 1I) and M2 macrophage populations and M2/M1 ratio in KD tumors (Fig. 1K). A higher ratio of M2/M1 macrophages in the TME is clinically associated with a poorer prognosis in CRC (25). Together, these results demonstrate that KD induces the reversal of an immunosuppressive TME.

Increased ketogenesis represses CXCL12 expression in CAFs

CAFs, a key constituent of the TME, promote immunosuppression in TME via secretion of chemokines such as CXCL12 (26). To determine how an increase in ketogenesis inhibits an immunosuppressive TME, we have established human primary CAFs, hCAF-05 and hCAF-6231 with inducible overexpression of HMGCS2. HMGCS2 expression in hCAF-05 cells was induced by treatment with DOX and RNA-seq analysis was performed. Overexpression of HMGCS2 decreased CXCL12 mRNA expression and increased βHB production in hCAF-05 without affecting the expression of CAF biomarkers ACTA2, S100A4 and MMP2 (27) (Supplementary Fig. 3A–C). Consistent with the results from RNA-seq analysis, overexpression of HMGCS2 in hCAF-05 and hCAF-6231 cells (Supplementary Fig. 3D) resulted in a marked decrease in the expression of CXCL12 mRNA (Fig. 2A; **left panel**), CXCL12 protein (SDF1) in cell lysates (Fig. 2B) and secretion in culture medium (Fig. 2C), as determined by RT-PCR and ELISA, respectively. In contrast, overexpression of HMGCS2-C166A (HMGCS2-Mut), an enzymatic dead HMGCS2 (17), did not affect either the expression of CXCL12 mRNA (Fig. 2A; **right panel**) and protein or the levels of βHB in cell lysates (Supplementary Fig. 3E). Moreover, βHB treatment significantly inhibited CXCL12 mRNA (Fig. 2D) and protein (Fig. 2E) expression in human primary CAFs (hCAF-05 and hCAF-6231) and mouse primary CAFs (mCAFs) (isolated from CT26 tumors). Consistently, reduced CXCL12 mRNA expression was found in mouse primary CAFs isolated from KD MC38 tumors (Fig. 2F). In contrast, treatment with βHB did not affect CXCL12 mRNA levels in human normal colon fibroblasts CCD-18Co (Supplementary Fig. 3F), suggesting a specific inhibition of CXCL12 expression in CAFs. As CXCL12, expressed in the TME mainly by CAFs (Supplementary Fig. 4) (7), plays a critical role in the immunosupressive TME (4), our results demonstrate that increased

ketogenesis overcomes the immunosupressive TME through the inhibition of CXCL12 expression.

KLF5 mediates the regulation of CXCL12 expression

Our RNA-seq analysis showed decreased KLF5 mRNA levels in CAFs with overexpression of HMGCS2 (Supplementary Fig. 3A). To further determine the inhibition of KLF5 expression by HMGCS2, HMGCS2 expression in hCAF-05-HMGCS2 cells was induced by treatment with DOX. As shown in Fig. 3A&B, overexpression of HMGCS2 significantly repressed KLF5 mRNA expression. Moreover, HMGCS2, but not HMGCS2-Mut, markedly repressed KLF5 protein expression without affecting KLF4 protein expression in hCAF-05 cells. In agreement with HMGCS2 overexpression, treatment of hCAF-05, hCAF-6231 and mCAFs with βHB significantly repressed the protein expression of KLF5, but not KLF4, in these CAFs (Fig. 3C). Recently, βHB has been shown to act as an endogenous inhibitor of class I histone deacetylases (HDACs) (28). βHB inhibited HDAC activity in CAFs as noted by the increased acetylation of histone H3 lysine 9 (H3K9ac). Moreover, treatment with sodium butyrate (NaBT), which inhibits class I HDACs (28), or MS-275, a selective HDAC1 inhibitor (29), or knockdown of HDAC1, repressed the protein expression of KLF5, but not KLF4, in hCAF-05 cells (Fig. 3C). These data demonstrate that an increase in ketogenesis inhibits KLF5 expression through the inhibition of HDAC1 in CAFs.

Next, we determined whether KLF5 regulates CXCL12 expression. Overexpression of KLF5 by infection with Ad-KLF5 significantly increased the expression of CXCL12 mRNA and protein compared to Ad-GFP control in hCAF-05 cells (Fig. 3D&E) and hCAF-6231 cells (Supplementary Fig. 5A–C). Moreover, βHB reduced CXCL12 mRNA and protein expression in control GFP hCAF-05 cells but not in KLF5 hCAF-05 cells (Fig. 3D; Supplementary Fig. 5D). In contrast, knockdown of KLF5 by transfection with siRNA targeting KLF5 (Fig. 3F) or inhibition of KLF5 by treatment with ML-264 (Fig. 3G), a selective KLF5 inhibitor (30), decreased CXCL12 mRNA expression in hCAF-05 cells. Moreover, knockdown of KLF5 repressed CXCL12 protein (SDF1) expression and secretion (Fig. 3H). These results demonstrate that an increase in ketogenesis represses CXCL12 expression through inhibition of KLF5 expression in CAFs.

KLF5 binds to GC-box sequence near the core promoter elements and amplifies transcription of its target genes (31). An essential binding site for KLF5 is 5'-GGGGTGGG-3' (31). We identified two KLF5 binding sites (motif 1 and motif 2) in the CXCL12 promoter (Fig. 3I). To determine whether KLF5 binds to CXCL12 promoter, we performed a Chromatin Immunoprecipitation (ChIP) assay. Crosslinked chromatin was prepared from hCAF-05 cells and immunoprecipitation was performed using either the anti-KLF5 antibody or IgG; the sequences containing no KLF5 binding site (negative control; upper row), the putative KLF5 binding site 1 (motif 1; middle row) and binding site 2 (motif 2; lower row) were amplified (Fig. 3J). We found that KLF5 mainly binds to the CXCL12 promoter region containing KLF5 binding motif 1; this binding was markedly attenuated by HMGCS2 overexpression. To determine whether KLF5 regulates CXCL12 expression through its binding to this KLF5 motif, we next cloned the CXCL12 promoter (Fig. 3K). hCAF-05 cells were transfected with CXCL12 promoter deletion constructs together with

control vector or a plasmid encoding KLF5 (Fig. 3L). Overexpression of KLF5 induced CXCL12 promoter activity with deletion of KLF5 binding site 1 resulting in a marked decrease in KLF5-induced CXCL12 promoter activation. Deletion of the two KLF5 binding sites eliminated KLF5 induction. Together, these results demonstrate that KLF5 regulates CXCL12 expression through promoter binding and activation.

Increased ketogenesis inhibits CAF growth

To determine whether an increase in ketogenesis affects CAF proliferation, hCAF-05, hCAF-6231 or mCAFs cells were treated with βHB for 6 days. As shown in Fig. 4A–C, βHB markedly inhibited the growth of these CAFs. Moreover, overexpression of HMGCS2 significantly repressed the proliferation of hCAF-05 cells (Fig. 4D). In agreement with the inhibition of proliferation, treatment with βHB induced cells to accumulate at the G0/G1 cell cycle checkpoint (Fig. 4E) and increased expression of p53 and $p21^{Waf1}$ in hCAF-05 cells (Fig. 4F). To determine the effect of KD on CAFs in MC38 and CT26 tumors, the expression of α-SMA, a marker of CAFs (27), was determined by western blot. Feeding a KD repressed the expression of α-SMA in MC38 and CT26 tumors (Fig. 4G&H). Together, these results demonstrate that increased ketogenesis inhibits CAF proliferation. Since βHB, at the same concentration that was used to treat CAFs, did not inhibit CRC cell proliferation (Supplementary Fig. 1), our results emphasize the functional effects of ketogenesis on the TME. To determine whether KLF5 contributes to CAF growth, hCAF-05 cells were infected with Ad-GFP or Ad-KLF5 followed by treatment with βHB. Overexpression of KLF5 increased hCAF-05 proliferation and reversed the inhibition of hCAF-05 cell proliferation by βHB treatment (Fig. 4I). In contrast, knockdown of KLF5 resulted in the inhibition of hCAF-05 cell proliferation (Fig. 4J). Together, our results demonstrate the regulation of CAF growth by the HMGCS2/βHB/KLF5 signaling axis.

Ketogenesis is downregulated in CRC patient samples

We have shown that increased ketogenesis inhibits KLF5-dependent CXCL12 expression and improves the immunosuppressive TME. We next determined the levels of βHB in human CRCs. As shown in Fig. 5A, the level of βHB was decreased in twelve of total thirteen tumor samples analyzed compared to the adjacent normal controls. Conversely, increased CXCL12 protein (SDF1) levels were noted in the CRCs (Fig. 5B). In agreement with the decreased βHB, decreased HMGCS2 protein levels were noted in eight of ten CRCs compared with matched normal colonic mucosa (Fig. 5C). High KLF5 expression is associated with poor prognosis in patients with CRC and liver metastasis (32). Moreover, elevated expression of CXCL12 protein (SDF1), CXCR4 and CXCR7 in CRCs has been reported (33,34). To further examine whether decreased expression of HMGCS2 was correlated with increased KLF5 and SDF1 expression in human CRCs, samples of 5 pair-matched CRCs with liver metastasis were analyzed using IHC staining. As shown in Fig. 5D, the intensity of HMGCS2 is negatively correlated with KLF5, SDF1, CXCR4 and CXCR7 in normal colon mucosa, primary and metastatic tumors, thus demonstrating that the decreased levels of HMGCS2/βHB are present in association with increased CXCL12/CXCR4/CXCR7 signaling in CRCs.

KD represses CXCL12 expression in tumors and enhances antitumor efficacy of anti-PD1 therapy

We showed that HMGCS2/βHB inhibits CXCL12 expression in CAFs. To next determine whether KD inhibits the expression of CXCL12 in tumors, BALB/cJ or C57BL/6J mice with subcutaneously implanted CT26 cells or MC38 tumors were fed a NC or KD for 14 days (Fig. 6A), and CXCL12 protein (SDF1) and βHB levels in plasma and tumors were determined. βHB production was markedly elevated in the plasma (Fig. 6B&D) and tumors (Fig. 6C&E) from mice fed with KD. Conversely, KD significantly repressed the levels of SDF1 in the plasma (Fig. 6B&D) and tumor tissues (Fig. 6C&E). As CXCL12 contributes to CRC resistance to ICB therapy (35), we next determined whether KD enhances the efficacy of anti-PD1 therapy (Fig. 6F). Administration of KD enhanced the antitumor effects of anti-PD1 therapy in CT26 (Fig. 6G) and MC38 (Fig. 6H) tumor models. These effects on tumor growth correlated well with the improved survival observed in the tumor bearing mice, establishing that anti-PD-1 antitumor activity is impaired with a decrease in ketogenesis but is restored with feeding a KD (Fig. 6I&J). CT26 tumor eradication was noted in 2/10 surviving mice in the group treated with anti-PD1. Importantly, tumor eradication was observed in all 7 surviving mice that received the combined KD and anti-PD1 antibody treatment.

KD inhibits CRC metastasis

Activation of CXCL12/CXCR4/CXCR7 signaling promotes tumor growth, migration, invasion, angiogenesis and metastasis in various cancers including CRCs (35). To test whether alteration of ketogenesis affects CRC cell migration and invasion, we used conditioned medium (CM) collected from cultures of CAFs that overexpress HMGCS2 or HMGCS2-Mut. CM from CAFs overexpressing HMGCS2 (Fig. 7A&B), but not HMGCS2-Mut (Supplementary Fig. 6A&B), inhibited migration and invasion of HCT116 cells compared with CM from CAFs with control vector as determined by Boyden chamber assays and by a scratch migration assay (Supplementary Fig. 6C). To determine whether KD inhibits cancer metastasis, we used an *in vivo* lung metastasis model (Fig. 7C), and lung metastasis was assessed by GFP imaging (Fig. 7D&E). Compared to NC, KD remarkably repressed lung metastases in mice. The most common metastatic sites of CRC are the liver and the lung. We next determined whether KD affects the levels of CXCL12 in lung and liver tissues. KD repressed the expression of SDF1, which was associated with an increase of βHB in lung (Fig. 7F&G) and liver (Supplementary Fig. 6D&E) tissues of mice bearing tumors. Taken together, these findings demonstrate that an increase in ketogenesis results in the inhibition of CRC cell migration, invasion, and metastasis.

Discussion

Metabolic reprogramming plays a critical role in the inhibition of antitumor immunity and thereby in tumor progression and metastasis (36). The TME is a critical factor that affects targeted therapies for CRCs (3). A KD has been demonstrated to be a safe and achievable component in the treatment strategy for some cancers (10,37). Recently, KDs have been shown to enhance the anticancer effects of ICB in CRC, melanoma, renal, and non-small cell lung cancer orthotopic tumor models (11,12). However, the activity of ketogenesis and the

role of ketogenesis on the immunosuppressive TME are not known. Interestingly, our current study uncovers a novel metabolic fitness and flexibility of the immunosuppressive TME in CRCs. We show that ketogenesis is downregulated in the TME; increased ketogenesis represses KLF5-dependent CXCL12 expression and improves immunosuppressive TME as noted by increased intratumoral $CD8^+$ T cell and NK cell infiltration in conjunction with decreased MDSC and M2-like macrophage populations in the TME, which leads to the enhanced efficacy of immunotherapy and inhibited lung metastasis (Fig. 7H). Importantly, our findings demonstrate that impaired ketogenesis in the TME is critical for CRC immune escape.

Our current study provides insight into the status of ketogenesis in the immunosuppressive TME. We show that KD inhibits MC38 tumor growth in immune competent mice while the ketone body βHB had minor effects on the proliferation of CRC cell lines suggesting that KD may inhibit tumor growth through the TME. Indeed, we found that ketogenesis is downregulated in CRCs and that feeding a KD inhibited the immunosuppressive TME. Our results are the first to show that downregulated ketogenesis in CRCs contributes to the immunosuppressive TME. Activation of CXCL12/CXCR4 induces the recruitment of immunosuppressive cells in the CRC TME (38). Moreover, CXCL12 promotes recruitment of other $CXCR4^+$ immunosuppressive cells such as MDSCs and regulatory T-cells (Tregs) toward the TME (4). Blocking CXCR4 and/or CXCR7 improves immunosuppressive TME, inhibits CRC lung metastasis, promotes infiltration of cytotoxic T cells and synergizes with anti-PD-1 therapy in murine CRC models (39–42). CXCL12 has been shown to suppress the proliferation of blood-derived NK cells (43). We showed that KD repressed CXCL12 expression, improved the immunosuppressive TME, and enhanced the efficacy of anti-PD1 therapy for CRCs. Our results suggest that KD may reduce the recruitment of $CXCR4^+$ immunosuppressive cells by repression of CXCL12 expression, thus allowing for increased cancer-specific NK and $CD8^+$ T cell infiltration and enhanced efficacy of ICB therapy for CRCs.

Although CXCL12 is increased in TME and is critical for tumor immunosuppression (9), regulation of CXCL12 in TME remains largely undefined. We demonstrated that an increase in ketogenesis (i.e., overexpression of HMGCS2, treatment with either βHB or KD) repressed the expression of CXCL12 through the inhibition of HDAC1-dependent KLF5 expression. CXCL12, which is expressed in the TME mainly by CAFs (7), plays a crucial role in the immunosuppressive TME. KLF5, a zinc-finger transcription factor that contributes to CRC cell growth (44), has recently been shown to inhibit intratumoral accumulation of cytotoxic T cells in pancreatic ductal adenocarcinoma (45). However, it is not known whether KLF5 contributes to the immunosuppression in CRCs. CXCL12 is upregulated in numerous cancers; however, very little is known regarding the mechanisms for this increase. Our data identifies CXCL12 as a direct target of KLF5, which binds to the CXCL12 promoter and transcriptionally controls CXCL12 expression in CAFs. Moreover, we show that an increase in ketogenesis or inhibition of KLF5 resulted in the inhibition of CAF proliferation. An increased percentage of tumor stromal cells, such as CAFs, is associated with a poor prognosis for CRC (5). Our results demonstrate that an increase in ketogenesis represses CXCL12 levels in the TME through both of inhibition of KLF5-dependent CXCL12 induction and inhibition of CAF proliferation. Our findings that KLF5

plays a critical role in promoting immunosuppressive TME in CRCs provide an important step in unraveling the precise molecular regulators of CXCL12 expression in cancer.

CXCL12 plays a critical role in cancer metastasis and is a potential target for developing effective therapeutics against metastatic cancers (7). Tumor cells expressing CXCR4 or CXCR7 migrate following a CXCL12 gradient; organs with high CXCL12 expression are common terminals of CXCL12-guided cell migration (46). In addition to primary tumors, there is also sufficient expression of CXCL12 in the bone marrow, lungs, lymph nodes and liver attracting CXCR4 positive cancer cells to these CXCL12-rich mesenchymal stroma niches to initiate metastasis (4). CXCL12 is mainly expressed by mesenchymal stromal cells in these organs (7). Moreover, there are number of reports demonstrating that mesenchymal stem cells (MSCs) can function as precursors for CAFs (47). We showed that increased ketogenesis inhibits CXCL12 expression in CAFs. These results suggest that increased ketogenesis may also repress CXCL12 in these MSCs. The most common metastatic sites of CRCs are the liver and the lung. Reduction of CXCL12 in liver stroma has been shown to reduce the potential of CRC liver metastasis (48). Moreover, cancerous and non-cancerous lung tissues showed increased expression of CXCL12 in CRC patients, suggesting a contribution of CXCL12 to this site of metastasis for CRCs (49). We showed that feeding a KD repressed CXCL12 expression in primary tumors, plasma, liver, and lung tissues, demonstrating the potential of using a supplemental KD to directly inhibit CXCL12 stimulation of cancer cells, thus interfering with the tumor immune response and the cancer biology driving the establishment of metastasis.

Hyper-activation of the CXCL12/CXCR4 axis is common in many solid tumors and plays a critical role in tumor immunosuppression and metastasis (9); therefore, the reduction of CXCL12 concentrations has the potential to inhibit the immunosuppressive TME and decrease tumor and immunosuppressive cell activation/migration within the primary tumor and metastatic niche.

Inhibition of the CXCR4/CXCL12 or CXCR7/CXCL12 axis is an attractive strategy for treatment of CRCs overexpressing these receptors (4). AMD3100 is an FDA-approved CXCR4 antagonist used for peripheral blood stem cell transplantation; however, its application to solid tumors is limited by its poor pharmacokinetics and toxic adverse effects after long-term administration (50). Thus, an alternative strategy to repress CXCL12 expression is necessary. Our findings provide a novel metabolic strategy to repress CXCL12 expression in the primary and metastatic niche, demonstrating a potential of using KD to enhance the efficacy of ICB for metastatic CRCs and thus increase overall survival. Since increased CXCL12 in the primary tumor and metastatic niche is a general phenomenon in a number of cancers, our findings suggest a potential benefit of using KD not only for CRCs but also for other cancers with increased CXCL12.

Supplementary Material

Refer to Web version on PubMed Central for supplementary material.

Acknowledgments

The authors thank Donna Gilbreath for manuscript preparation; Dana Napier for tissue preparation, sectioning, and staining; Siva Gandhapudi and Jerry Woodward for Flow Cytometric analysis; the Flow Cytometry & Immune Monitoring core, OncoGenomics Shared Resource, Biospecimen Procurement and Translational Pathology, and Biostatistics and Bioinformatics Shared Resource Facilities of the University of Kentucky Markey Cancer Center (supported by National Cancer Institute grant P30 CA177558).

Financial Support:

This work was supported by National Institutes of Health grants R01 DK48498 and P30 CA177558 (to BME), and a pilot grant from P20 GM121327 (to QW).

References

1. Van Cutsem E, Cervantes A, Adam R, Sobrero A, Van Krieken JH, Aderka D, et al. ESMO consensus guidelines for the management of patients with metastatic colorectal cancer. Annals of oncology : official journal of the European Society for Medical Oncology 2016;27:1386–422 [PubMed: 27380959]
2. Ciardiello D, Vitiello PP, Cardone C, Martini G, Troiani T, Martinelli E, et al. Immunotherapy of colorectal cancer: Challenges for therapeutic efficacy. Cancer treatment reviews 2019;76:22–32 [PubMed: 31079031]
3. Gallo G, Vescio G, De Paola G, Sammarco G. Therapeutic Targets and Tumor Microenvironment in Colorectal Cancer. J Clin Med 2021;10
4. Mortezaee K. CXCL12/CXCR4 axis in the microenvironment of solid tumors: A critical mediator of metastasis. Life Sci 2020;249:117534 [PubMed: 32156548]
5. Musa M, Ali A. Cancer-associated fibroblasts of colorectal cancer and their markers: updates, challenges and translational outlook. Future Oncol 2020;16:2329–44 [PubMed: 32687721]
6. Barrett R, Puré E. Cancer-associated fibroblasts: key determinants of tumor immunity and immunotherapy. Current opinion in immunology 2020;64:80–7 [PubMed: 32402828]
7. Guo F, Wang Y, Liu J, Mok SC, Xue F, Zhang W. CXCL12/CXCR4: a symbiotic bridge linking cancer cells and their stromal neighbors in oncogenic communication networks. Oncogene 2016;35:816–26 [PubMed: 25961926]
8. Jung K, Heishi T, Incio J, Huang Y, Beech EY, Pinter M, et al. Targeting CXCR4-dependent immunosuppressive Ly6C(low) monocytes improves antiangiogenic therapy in colorectal cancer. Proceedings of the National Academy of Sciences of the United States of America 2017;114:10455–60 [PubMed: 28900008]
9. Santagata S, Ieranò C, Trotta AM, Capiluongo A, Auletta F, Guardascione G, et al. CXCR4 and CXCR7 Signaling Pathways: A Focus on the Cross-Talk Between Cancer Cells and Tumor Microenvironment. Frontiers in oncology 2021;11:591386 [PubMed: 33937018]
10. Tan-Shalaby J. Ketogenic Diets and Cancer: Emerging Evidence. Fed Pract 2017;34:37s–42s
11. Dai X, Bu X, Gao Y, Guo J, Hu J, Jiang C, et al. Energy status dictates PD-L1 protein abundance and anti-tumor immunity to enable checkpoint blockade. Mol Cell 2021
12. Ferrere G, Tidjani Alou M, Liu P, Goubet AG, Fidelle M, Kepp O, et al. Ketogenic diet and ketone bodies enhance the anticancer effects of PD-1 blockade. JCI Insight 2021;6
13. Wang Q, Zhou Y, Rychahou P, Fan TW, Lane AN, Weiss HL, et al. Ketogenesis contributes to intestinal cell differentiation. Cell Death Differ 2017;24:458–68 [PubMed: 27935584]
14. Kim JT, Li C, Weiss HL, Zhou Y, Liu C, Wang Q, et al. Regulation of Ketogenic Enzyme HMGCS2 by Wnt/beta-catenin/PPARgamma Pathway in Intestinal Cells. Cells 2019;8
15. Rychahou P, Bae Y, Reichel D, Zaytseva YY, Lee EY, Napier D, et al. Colorectal cancer lung metastasis treatment with polymer-drug nanoparticles. J Control Release 2018;275:85–91 [PubMed: 29421609]
16. Ringel AE, Drijvers JM, Baker GJ, Catozzi A, García-Cañaveras JC, Gassaway BM, et al. Obesity Shapes Metabolism in the Tumor Microenvironment to Suppress Anti-Tumor Immunity. Cell 2020

17. Vilà-Brau A, De Sousa-Coelho AL, Mayordomo C, Haro D, Marrero PF. Human HMGCS2 regulates mitochondrial fatty acid oxidation and FGF21 expression in HepG2 cell line. J Biol Chem 2011;286:20423–30 [PubMed: 21502324]

18. Li C, Zhou Y, Kim JT, Sengoku T, Alstott MC, Weiss HL, et al. Regulation of SIRT2 by Wnt/β-catenin signaling pathway in colorectal cancer cells. Biochim Biophys Acta Mol Cell Res 2021;1868:118966 [PubMed: 33450304]

19. Wang Q, Zhou Y, Rychahou P, Harris JW, Zaytseva YY, Liu J, et al. Deptor Is a Novel Target of Wnt/beta-Catenin/c-Myc and Contributes to Colorectal Cancer Cell Growth. Cancer Res 2018;78:3163–75 [PubMed: 29666061]

20. Huang X, Ye Q, Chen M, Li A, Mi W, Fang Y, et al. N-glycosylation-defective splice variants of neuropilin-1 promote metastasis by activating endosomal signals. Nat Commun 2019;10:3708 [PubMed: 31420553]

21. Ringel AE, Drijvers JM, Baker GJ, Catozzi A, Garcia-Canaveras JC, Gassaway BM, et al. Obesity Shapes Metabolism in the Tumor Microenvironment to Suppress Anti-Tumor Immunity. Cell 2020;183:1848–66 e26 [PubMed: 33301708]

22. Arlauckas SP, Garren SB, Garris CS, Kohler RH, Oh J, Pittet MJ, et al. Arg1 expression defines immunosuppressive subsets of tumor-associated macrophages. Theranostics 2018;8:5842–54 [PubMed: 30613266]

23. Tay RE, Richardson EK, Toh HC. Revisiting the role of CD4(+) T cells in cancer immunotherapy-new insights into old paradigms. Cancer Gene Ther 2021;28:5–17 [PubMed: 32457487]

24. Nelson MA, Ngamcherdtrakul W, Luoh SW, Yantasee W. Prognostic and therapeutic role of tumor-infiltrating lymphocyte subtypes in breast cancer. Cancer Metastasis Rev 2021;40:519–36 [PubMed: 33963482]

25. Inagaki K, Kunisho S, Takigawa H, Yuge R, Oka S, Tanaka S, et al. Role of tumor-associated macrophages at the invasive front in human colorectal cancer progression. Cancer science 2021;112:2692–704 [PubMed: 33964093]

26. Liu T, Han C, Wang S, Fang P, Ma Z, Xu L, et al. Cancer-associated fibroblasts: an emerging target of anti-cancer immunotherapy. Journal of hematology & oncology 2019;12:86 [PubMed: 31462327]

27. Han C, Liu T, Yin R. Biomarkers for cancer-associated fibroblasts. Biomark Res 2020;8:64 [PubMed: 33292666]

28. Shimazu T, Hirschey MD, Newman J, He W, Shirakawa K, Le Moan N, et al. Suppression of oxidative stress by beta-hydroxybutyrate, an endogenous histone deacetylase inhibitor. Science 2013;339:211–4 [PubMed: 23223453]

29. Khan N, Jeffers M, Kumar S, Hackett C, Boldog F, Khramtsov N, et al. Determination of the class and isoform selectivity of small-molecule histone deacetylase inhibitors. Biochem J 2008;409:581–9 [PubMed: 17868033]

30. Bialkowska A, Crisp M, Madoux F, Spicer T, Knapinska A, Mercer B, et al. ML264: An Antitumor Agent that Potently and Selectively Inhibits Krüppel-like Factor Five (KLF5) Expression: A Probe for Studying Colon Cancer Development and Progression. Probe Reports from the NIH Molecular Libraries Program. Bethesda (MD): National Center for Biotechnology Information (US); 2010.

31. Zhang X, Choi PS, Francis JM, Gao GF, Campbell JD, Ramachandran A, et al. Somatic Superenhancer Duplications and Hotspot Mutations Lead to Oncogenic Activation of the KLF5 Transcription Factor. Cancer Discov 2018;8:108–25 [PubMed: 28963353]

32. Takagi Y, Sakai N, Yoshitomi H, Furukawa K, Takayashiki T, Kuboki S, et al. High expression of Krüppel-like factor 5 is associated with poor prognosis in patients with colorectal cancer. Cancer science 2020;111:2078–92 [PubMed: 32279400]

33. Song ZY, Wang F, Cui SX, Gao ZH, Qu XJ. CXCR7/CXCR4 heterodimer-induced histone demethylation: a new mechanism of colorectal tumorigenesis. Oncogene 2019;38:1560–75 [PubMed: 30337690]

34. Yoshitake N, Fukui H, Yamagishi H, Sekikawa A, Fujii S, Tomita S, et al. Expression of SDF-1 alpha and nuclear CXCR4 predicts lymph node metastasis in colorectal cancer. Br J Cancer 2008;98:1682–9 [PubMed: 18443596]

35. Xu D, Li R, Wu J, Jiang L, Zhong HA. Drug Design Targeting the CXCR4/CXCR7/CXCL12 Pathway. Curr Top Med Chem 2016;16:1441–51 [PubMed: 26369824]
36. Martinez-Outschoorn UE, Peiris-Pages M, Pestell RG, Sotgia F, Lisanti MP. Cancer metabolism: a therapeutic perspective. Nature reviews Clinical oncology 2017;14:11–31
37. Khodadadi S, Sobhani N, Mirshekar S, Ghiasvand R, Pourmasoumi M, Miraghajani M, et al. Tumor Cells Growth and Survival Time with the Ketogenic Diet in Animal Models: A Systematic Review. International journal of preventive medicine 2017;8:35 [PubMed: 28584617]
38. Yu X, Wang D, Wang X, Sun S, Zhang Y, Wang S, et al. CXCL12/CXCR4 promotes inflammation-driven colorectal cancer progression through activation of RhoA signaling by sponging miR-133a-3p. Journal of experimental & clinical cancer research : CR 2019;38:32 [PubMed: 30678736]
39. Biasci D, Smoragiewicz M, Connell CM, Wang Z, Gao Y, Thaventhiran JED, et al. CXCR4 inhibition in human pancreatic and colorectal cancers induces an integrated immune response. Proc Natl Acad Sci U S A 2020;117:28960–70 [PubMed: 33127761]
40. D'Alterio C, Buoncervello M, Ieranò C, Napolitano M, Portella L, Rea G, et al. Targeting CXCR4 potentiates anti-PD-1 efficacy modifying the tumor microenvironment and inhibiting neoplastic PD-1. Journal of experimental & clinical cancer research : CR 2019;38:432 [PubMed: 31661001]
41. Zeelenberg IS, Ruuls-Van Stalle L, Roos E. The chemokine receptor CXCR4 is required for outgrowth of colon carcinoma micrometastases. Cancer Res 2003;63:3833–9 [PubMed: 12839981]
42. Guillemot E, Karimdjee-Soilihi B, Pradelli E, Benchetrit M, Goguet-Surmenian E, Millet MA, et al. CXCR7 receptors facilitate the progression of colon carcinoma within lung not within liver. Br J Cancer 2012;107:1944–9 [PubMed: 23169289]
43. Correia AL, Guimaraes JC, Auf der Maur P, De Silva D, Trefny MP, Okamoto R, et al. Hepatic stellate cells suppress NK cell-sustained breast cancer dormancy. Nature 2021
44. Ghaleb AM, Yang VW. The Pathobiology of Krüppel-like Factors in Colorectal Cancer. Current colorectal cancer reports 2008;4:59–64 [PubMed: 18504508]
45. Li J, Yuan S, Norgard RJ, Yan F, Sun YH, Kim IK, et al. Epigenetic and transcriptional control of the epidermal growth factor receptor (EGFR) regulates the tumor immune microenvironment in pancreatic cancer. Cancer Discov 2020
46. Bleul CC, Fuhlbrigge RC, Casasnovas JM, Aiuti A, Springer TA. A highly efficacious lymphocyte chemoattractant, stromal cell-derived factor 1 (SDF-1). The Journal of experimental medicine 1996;184:1101–9 [PubMed: 9064327]
47. Peng Y, Li Z, Li Z. GRP78 secreted by tumor cells stimulates differentiation of bone marrow mesenchymal stem cells to cancer-associated fibroblasts. Biochem Biophys Res Commun 2013;440:558–63 [PubMed: 24113381]
48. Benedicto A, Romayor I, Arteta B. CXCR4 receptor blockage reduces the contribution of tumor and stromal cells to the metastatic growth in the liver. Oncol Rep 2018;39:2022–30 [PubMed: 29436696]
49. Wang M, Yang X, Wei M, Wang Z. The Role of CXCL12 Axis in Lung Metastasis of Colorectal Cancer. Journal of Cancer 2018;9:3898–903 [PubMed: 30410593]
50. Song JS, Chang CC, Wu CH, Dinh TK, Jan JJ, Huang KW, et al. A highly selective and potent CXCR4 antagonist for hepatocellular carcinoma treatment. Proc Natl Acad Sci U S A 2021;118

Statement of Significance

This study identifies ketogenesis as a critical regulator of the tumor microenvironment in colorectal cancer and suggests the potential for ketogenic diets as a metabolic strategy to overcome immunosuppression and prolong survival.

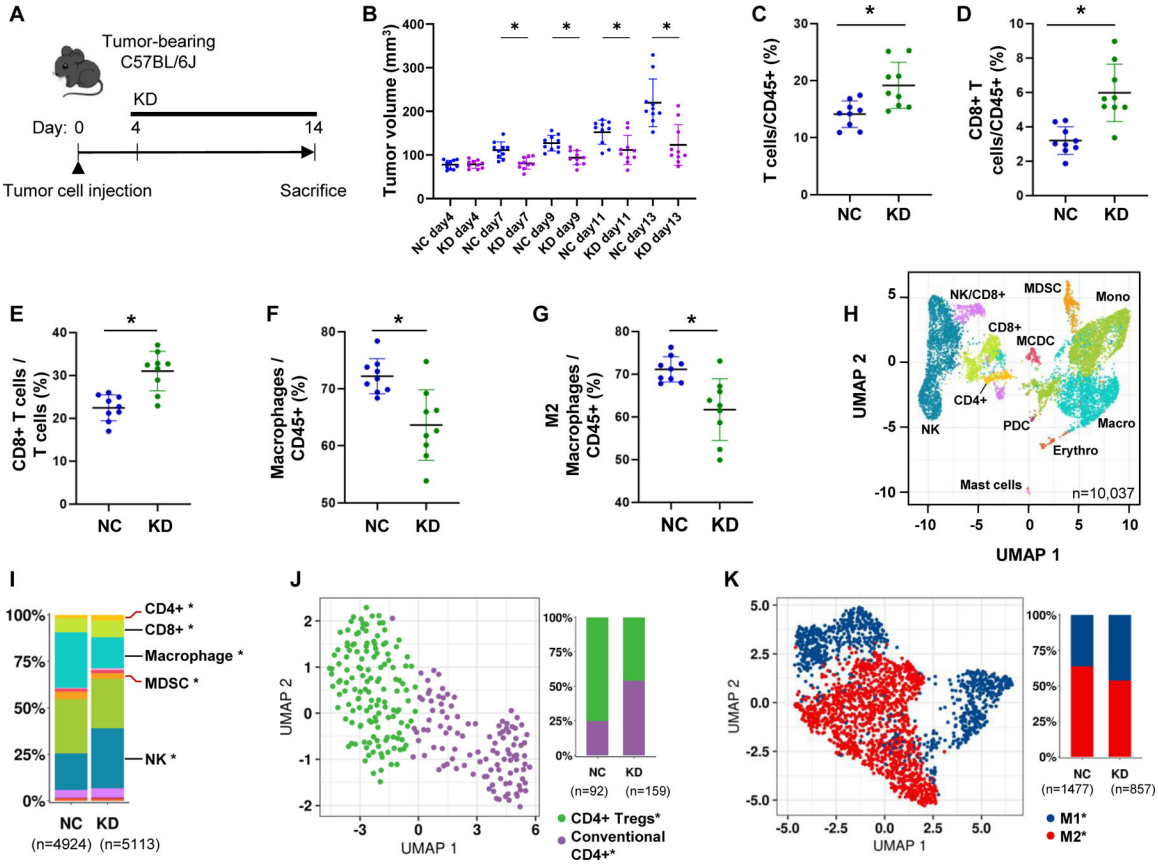

Fig. 1. KD reduces the accumulation of immunosuppressive cells and increases the population of NK and T cells in the TME.

(A) Schematic of mouse treatment. **(B)** Tumor growth curves of C57BL/6J mice fed NC or KD implanted with MC38 ($n = 10$ mice per group, $*p < 0.05$). **(C-G)** Quantification of tumor-infiltrating immune ($CD45^+$) cells in NC and KD MC38 tumors, assessed by flow cytometry and analyzed by FlowJo. Cell populations were identified as T cells ($CD45^+CD3^+$), $CD8^+$ T cells ($CD45^+CD3^+CD8a^+CD4^-$), macrophages ($CD45^+CD11b^+F4/80^+$) and M2 macrophages ($CD45^+CD11b^+F4/80^+CD206^+$) ($n = 9$ mice per group; $*p < 0.05$). **(H-K)** scRNA-seq analysis of tumor-infiltrating immune cell populations. Uniform manifold approximation and projection (UMAP) embeddings of scRNA-seq profiles from $CD45^+$ leukocyte cells showing cell types identified by integrated analysis (n=4924 cells from 5 pooled NC mice and n=5113 cells from 5 pooled KD mice). (H) Identification of tumor-infiltrating immune cell populations. NK/$CD8^+$: $CD8^+$ natural killer cells; MDSC: myeloid-derived suppressor cells; Mono: monocyte; $CD8^+$: $CD8^+$ T cells; $CD4^+$: $CD4^+$ T cells; MCDC: mature classic dendritic cells; NK: natural killer cells; PDC: plasmacytoid dendritic cells; Macro: macrophage; Erythro: erythrocytes. **(I-K)** Proportional differences in all leukocytes (I), (*FDR < 0.05), $CD4^+$ (J) and macrophage (K) infiltrate ($*p < 0.05$) from KD versus NC tumors.

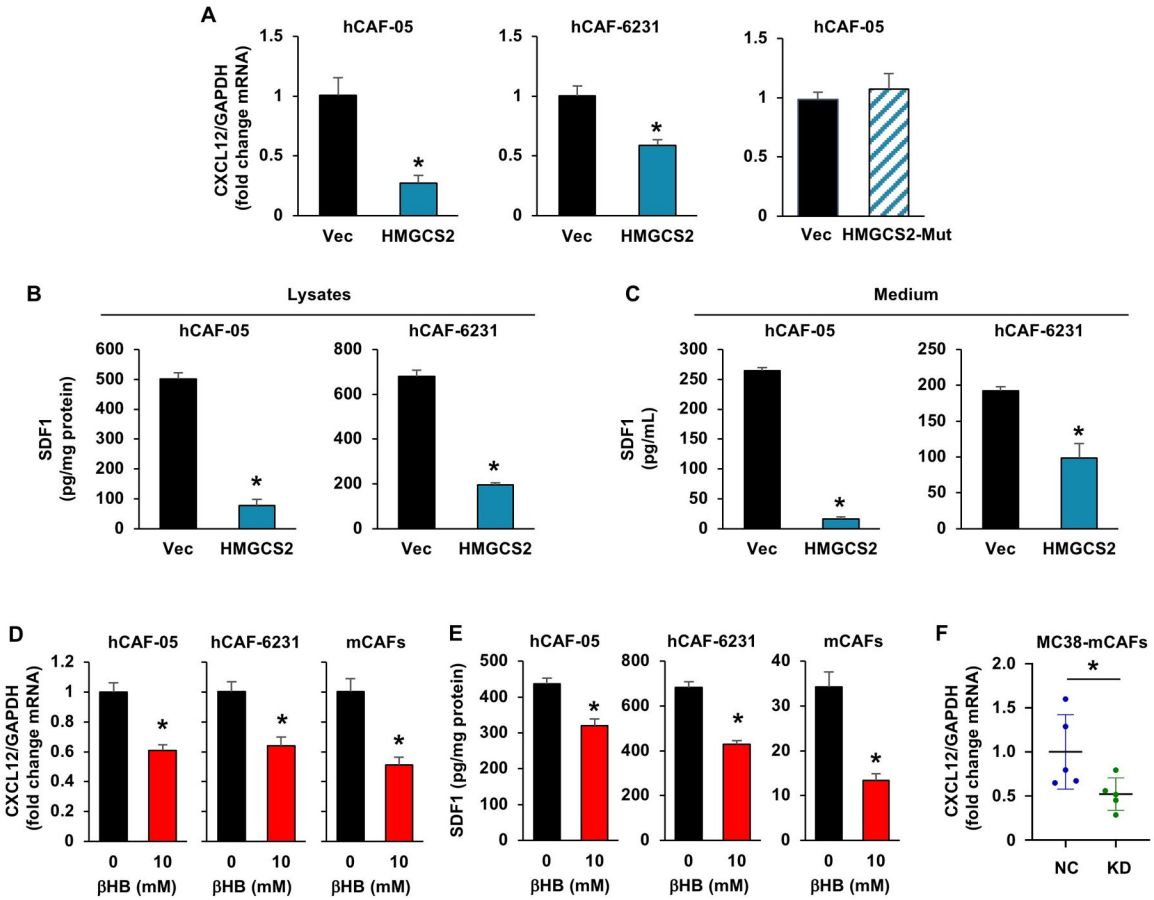

Fig. 2. Increase in ketogenesis represses CXCL12 expressions in CAFs.

(A) CXCL12 mRNA levels in human CAFs with or without HMGCS2 or HMGCS2-Mut overexpression were determined by real time RT-PCR. **(B-C)** SDF1 levels in cell lysates (B) or secreted in medium (C) were determined using an ELISA kit. **(D-E)** CAFs were treated with or without βHB (10 mM) for 48 h. CXCL12 mRNA levels (D) were determined by real time RT-PCR. SDF1 levels in cell lysates (E) were determined using an ELISA kit. Data are represented as mean ± SD. n=3, *p<0.05. Data are from 1 of 3 independent experiments with similar results. **(F)** Four days after MC38 cell implantation, C57BL/6J mice bearing established MC38 xenografts were fed with NC (n = 5 mice) or KD (n = 5 mice) for 14 days. Mouse CAFs were isolated from NC and KD tumors. CXCL12 mRNA levels in CAFs were determined by real time RT-PCR. *p<0.05.

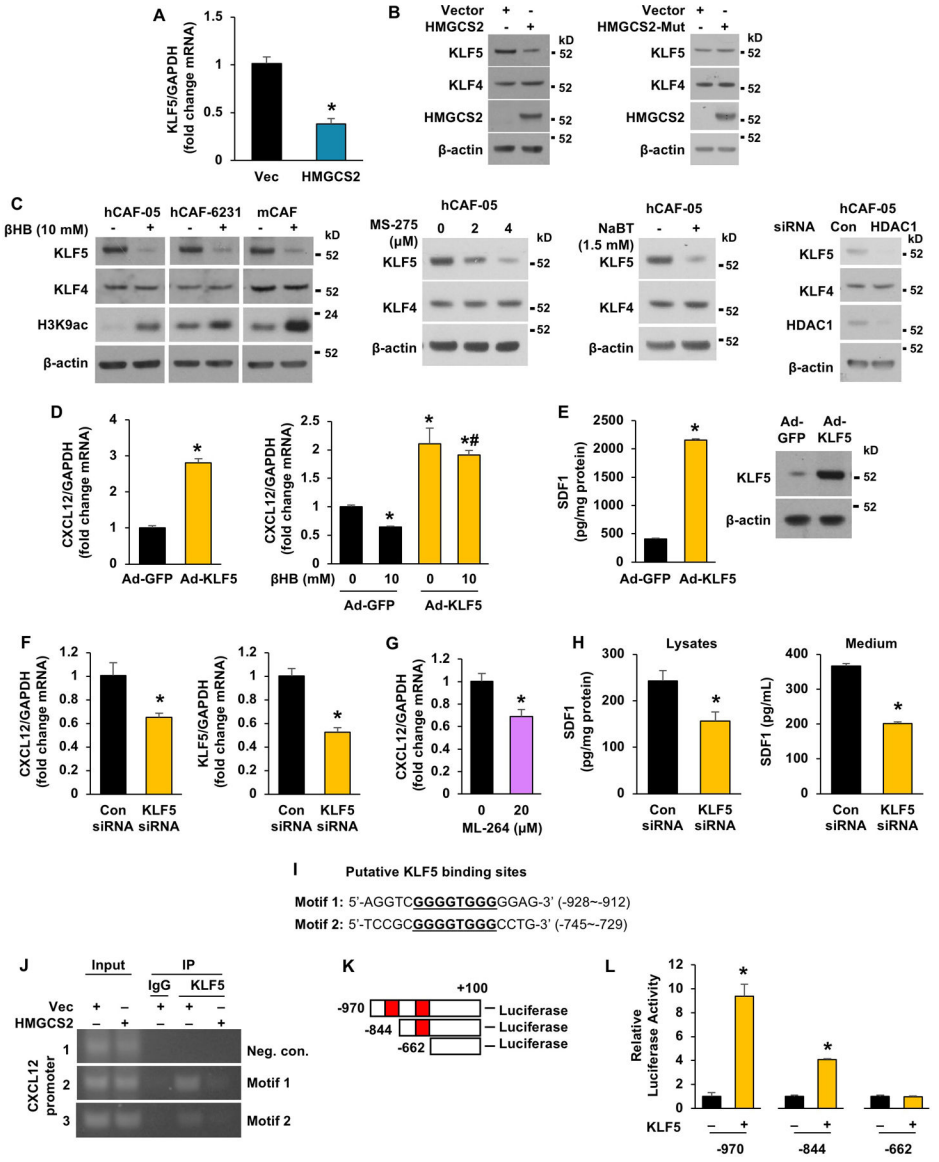

Fig. 3. KLF5 mediates the regulation of CXCL12 expression.

(A-B) Real time RT-PCR analysis of KLF5 mRNA (A) and western blot (B) analysis of KLF5, KLF4, HMGCS2 and β-actin expression in hCAF-05 cells with vector control or construct overexpressing HMGCS2 or HMGCS2-Mut. **(C)** Western blot analysis of KLF5, KLF4, H3K9ac, HDAC1 and β-actin expression in CAFs with or without either βHB or MS-275 or NaBT treatment for 48 h or knockdown of HDAC1. **(D)** Real time RT-PCR analysis of CXCL12 mRNA expression in hCAF-05 cells infected with Ad-GFP or Ad-KLF5 with or without βHB treatment for 48 h. **(E)** SDF1 expression in hCAF-05 cells infected with Ad-GFP or Ad-KLF5 was determined using an ELISA kit. KLF5 protein expression was determined by western blot. **(F-G)** Real time RT-PCR analysis of CXCL12 and KLF5 mRNA levels in hCAF-05 with knockdown (F) or inhibition (G) of KLF5. **(H)** Effects of KLF5 knockdown on SDF1 levels in CAF cell lysates or secreted in medium determined using an ELISA kit. **(I)** Promoter region of CXCL12 promoter with putative

KLF5 binding sites. **(J)** ChIP-PCR validation of KLF5 binding to the CXCL12 promoter. **(K)** CXCL12 promoter cloning. **(L)** Effects of KLF5 on CXCL12 promoter activity. Data are represented as mean ± SD; n=3, *$p<0.05$. Data are from 1 of 3 independent experiments with similar results.

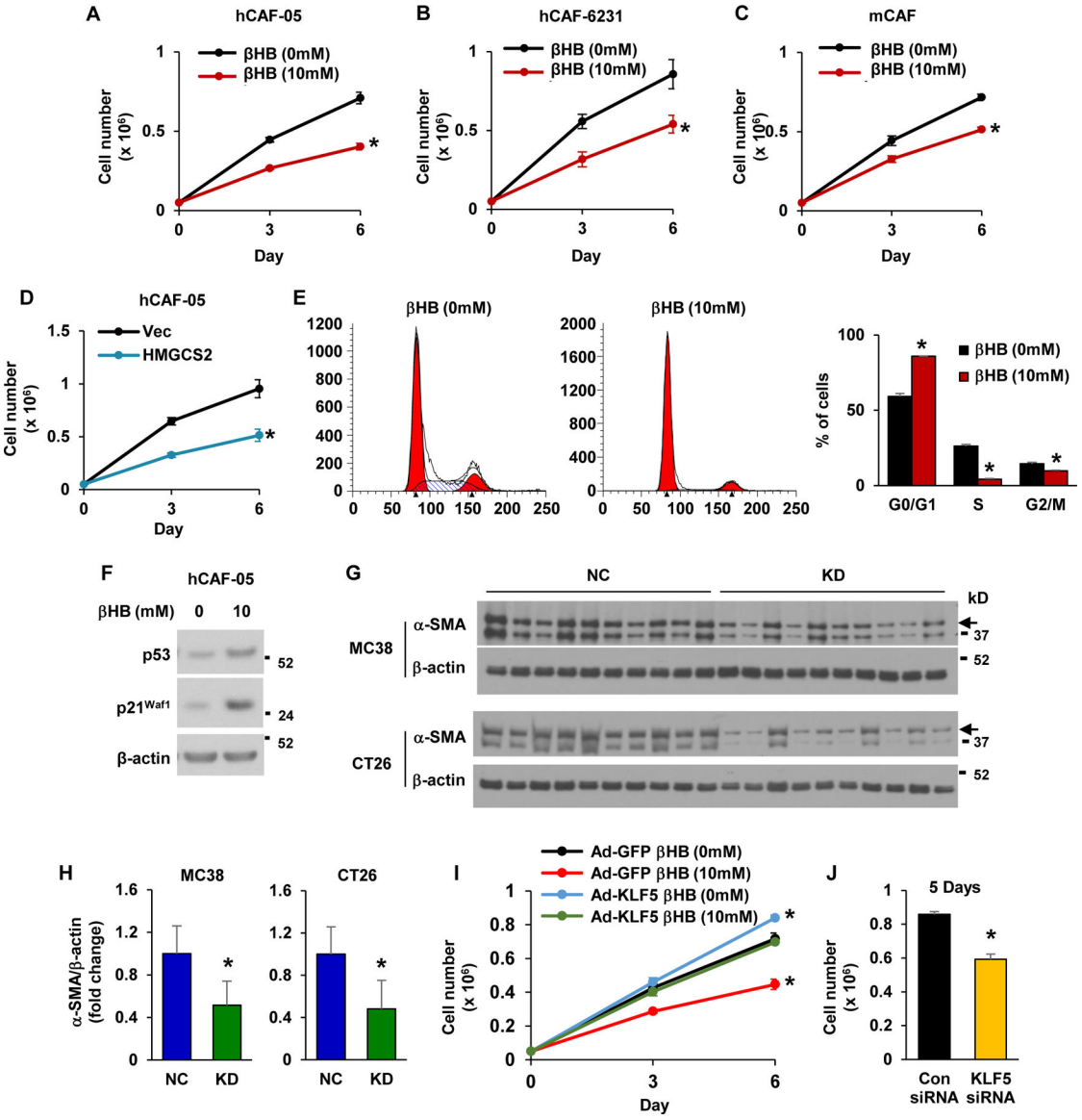

Fig. 4. Increase in ketogenesis inhibits CAF growth.

(A-D) hCAF-05 (A), hCAF-6231 (B) and mCAF (C) were treated with βHB. hCAF-05 cells with construct encoding HMGCS2 or vector control were treated with DOX (D). Cell proliferations were assessed over 6 days. Data are represented as mean ± SD; n=3, **p*<0.05. Data are from 1 of 3 independent experiments with similar results. (**E-F**) hCAF-05 cells were treated with or without βHB (10 mM) for 48 h. The percentage of cells in each phase of the cell cycle was determined by FACS (E). Data are represented as mean ± SD; n=3, **p*<0.05. Western blot analysis of p53 and $p21^{Waf1}$ protein expression (F). **(G-H)** The expression of α-SMA in MC38 and CT26 tumors from mice fed NC or KD for 14 days were analyzed by western blot (E). Each well represents a different mouse from the relevant group. α-SMA signals from 10 mice in each group were quantitated densitometrically and expressed as fold change with respect to total b-actin (F). Data are represented as mean ± SD. *p<0.05 vs NC. **(I)** hCAF-05 cells infected with Ad-GFP or Ad-KLF5 were treated

with or without βHB (10 mM) for 3 d or 6d. Cell proliferations were assessed. Data are represented as mean ± SD; n=3, *p<0.05 vs Ad-GFP. **(J)** The effect of KLF5 knockdown on growth of hCAF-05 cells. Data are represented as mean ± SD; n=3, *p<0.05. Data are from 1 of 3 independent experiments with similar results.

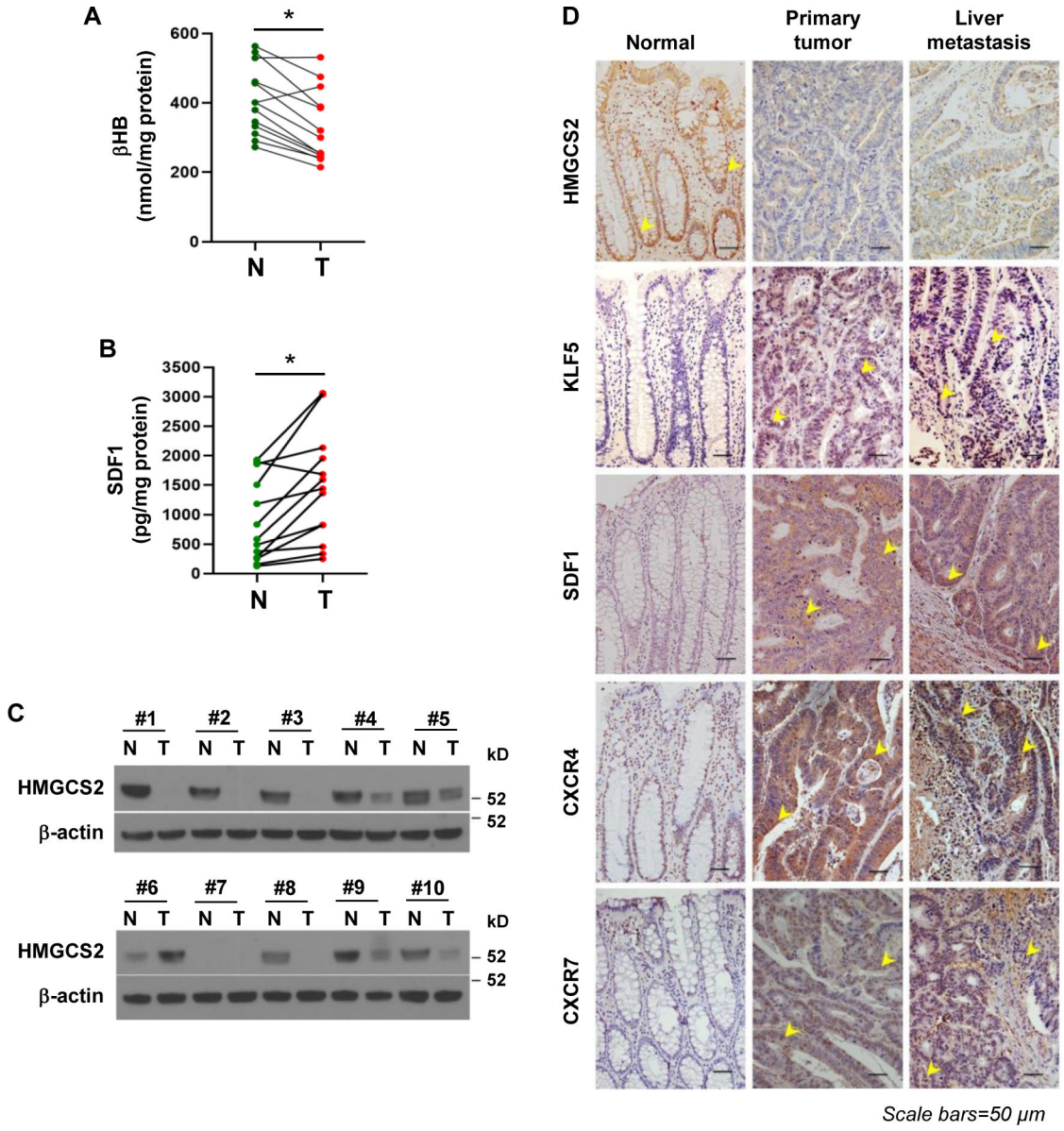

Fig. 5. Ketogenesis is downregulated in CRC patient samples.

(A-B) βHB levels (A) and SDF1 protein levels (B) in pair-matched human CRC tissues (T) and adjacent normal tissues (N) were determined using a βHB assay kit or an ELISA assay kit; n=13, **p*<0.05. **(C)** Expression of HMGCS2 in matched normal and tumor tissues from CRC patients were analyzed by western blot. **(D)** Representative IHC images taken from 5 pair-matched human CRC tissues stained with the antibodies against HMGCS2, KLF5, SDF1, CXCR4 and CXCR7 (arrows). Scale bars, 50 μm.

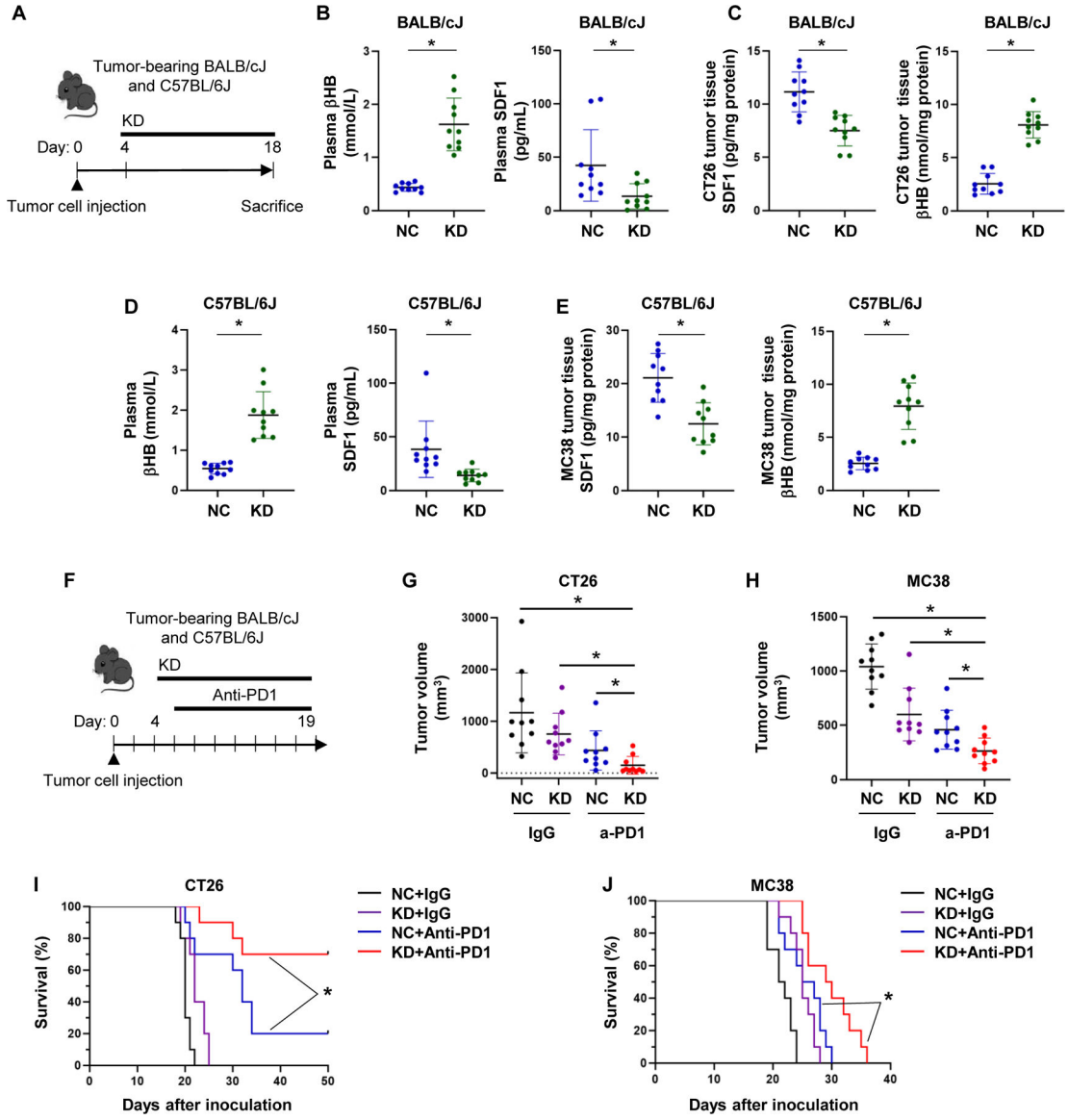

Fig. 6. KD enhanced antitumor efficacy of anti-PD1 therapy.

(A-E) Effects of KD on the levels of βHB and SDF1 in serum and MC38 and CT26 tumor tissues. (A) Schematic depicting experimental setup. (B-E) βHB levels and SDF1 protein levels in plasma (B, D) and tumor tissues (C, E) from BALB/cJ or C57BL/6J mice were determined using a βHB assay kit or an ELISA assay kit ($n = 10$ mice per group, $^*p < 0.05$). **(F)** Schematic depicting antitumor experiment. MC38 and CT26 cells (0.5×10^6) were injected subcutaneously into the flanks of C57BL/6J and BALB/cJ mice at day 0, respectively. When tumors grew to ~100 mm^3 by day 4, tumor-bearing mice were treated with KD alone or in combination with either anti-PD-1 antibody or IgG isotype control. Anti-PD-1 antibody (200 μg/injection) or IgG isotype control (200 μg/injection) were given on days 5, 7, 9, 11, 13, 15 and 17 after tumor inoculation by intraperitoneal (ip) injections. **(G-H)** Tumor volume of CT26 (G) and MC38 (H) tumors in BALB/cJ or C57BL/6J mice in different treatment groups at Day 18 as indicated in F ($n = 10$ mice per group, $^*p < 0.05$).

(I-J) Survival of BALB/cJ mice (I) with CT26 tumors and C57BL/6J mice (J) with MC38 tumors and treated as indicated in F; *$p < 0.05$ vs. NC plus anti-PD-1.

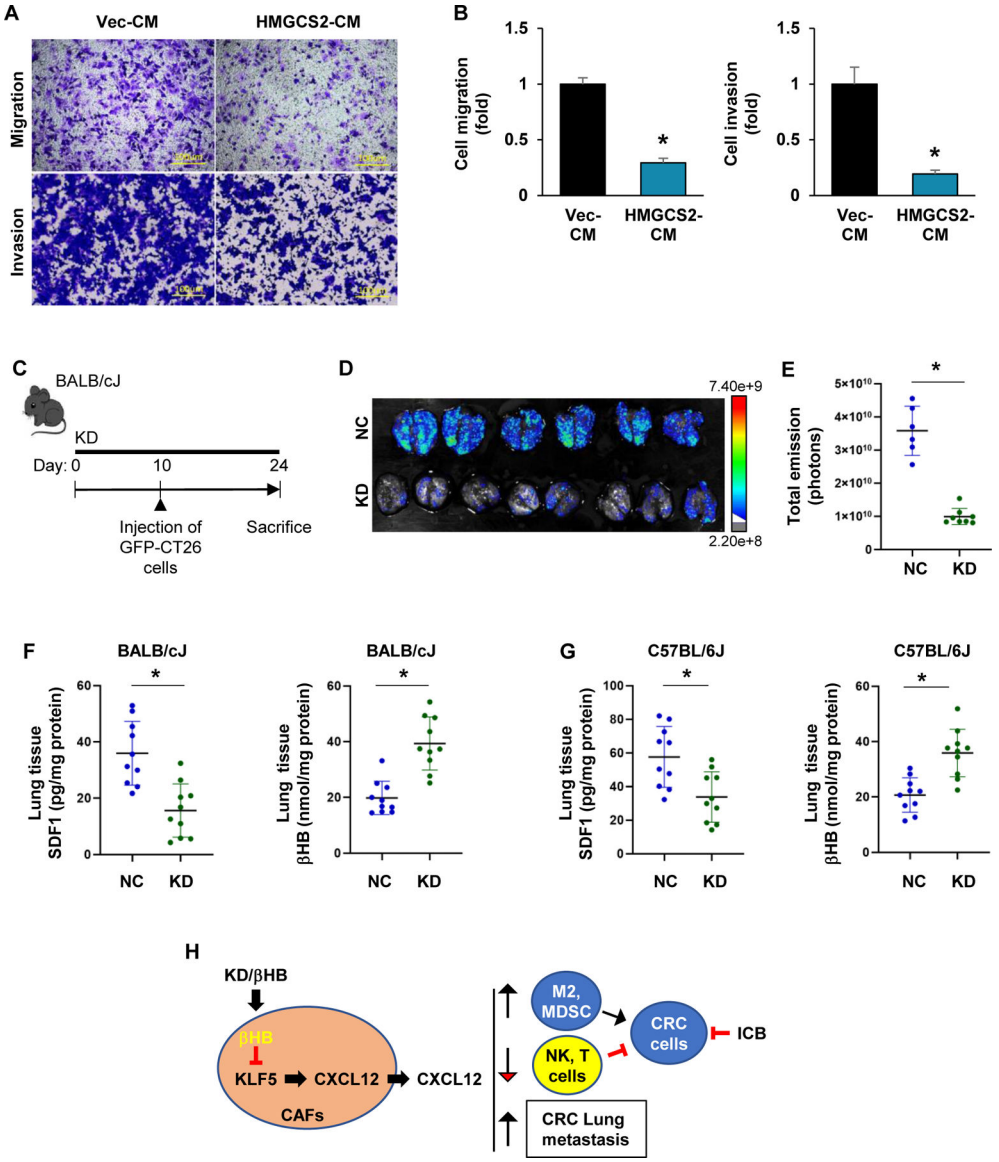

Fig. 7. KD inhibits CRC metastasis.

(A-B) Migration and invasion of HCT116 cells toward conditioned medium (CM) from cultured primary hCAF-05 cells overexpressing HMGCS2 compared with vector control, were evaluated using *in vitro* transwell migration and invasion assays in triplicate. The number of migrated and invaded cells per field ($n = 5$) were counted and expressed as a fold change compared with vector control; $*p < 0.05$ vs. vector control. Data are represented as mean ± SD. Data are from 1 of 3 independent experiments with similar results. **(C-E)** Effects of KD on CT26 cell lung metastasis. (C) Schematic of mouse treatment. (D) GFP imaging of lung metastasis in BALB/cJ mice; lung metastasis was established with intravenous injection of GFP-CT26 cells. (E) Quantitative analysis of luminescence in lung metastasis as shown in D was performed, and the results are presented as mean ± SD ($n = 6–8$ mice/group; $*p < 0.05$). **(F-G)** Effects of KD on the levels of βHB and SDF1 in lung tissues. Lung tissues from BALB/cJ (F) or C57BL/6J (G) mice treated in Fig. 6A were

harvested and βHB levels and SDF1 protein levels were determined using a βHB assay kit or an ELISA assay kit ($n = 10$ mice per group, $*p < 0.05$). **(H)** Increased ketogenesis enhances tumor immune response and inhibits lung metastasis through repression of KLF5-dependent CXCl12 expression. Model proposed to explain the KD enhanced antitumor efficacy of anti-PD1 treatment and inhibited lung metastasis.